Proceedings of the ASME 2020 International Design Engineering Technical Conferences &
Dynamic Systems and Control Conference
DSCC 2020
October 4-7, 2020, Pittsburgh, USA

DSCC2020-3254

DRAFT: THE EFFECT OF TIME DELAY ON THE STABILITY CONTROL OF TRAILERS

Hanna Zs. Horvath*
Department of Applied Mechanics
Budapest University of Technology and Economics
Budapest, 1111
Hungary
Email: hanna.horvath@mm.bme.hu

Denes Takacs
MTA-BME Research Group on Dynamics
of Machines and Vehicles
Budapest, 1111
Hungary
takacs@mm.bme.hu

ABSTRACT

The instability of the car-trailer systems very often leads to the snaking and/or rocking motions of trailers. In order to reduce the safety risk of these unwanted vibrations, stability control can be applied. In this paper, we use a spatial trailer model to analyze the effect of a possible control algorithm, which actuates by means of braking. For the sake of simplicity, the dynamics of the towing vehicle is modeled by the lateral displacement of the tow hitch that is supported laterally by a spring and damper. The longitudinal speed of the vehicle is kept constant. The effect of the braking forces are emulated in our study via a control torque, which is proportional to the yaw angle and the yaw rate. The time delay of the controller is also considered. Linear stability charts are constructed in the plane of the different system parameters. Linearly stable and unstable parameter domains are identified both for the vertical position of the center of gravity and the control gains. Numerical simulations are used to validate the theoretical results.

INTRODUCTION

The lateral stability problems of vehicles are in focus in the literature long time ago. Mechanical models with different complexity are constructed and widely used to analyze different phenomena in vehicle dynamics. The shimmy motion of steered wheels [1, 2], wobble motion of motorbikes [3] and snaking/rocking motion of trailers [4–7] are also current topics even nowadays.

Unfortunately, no universal solutions exist for the above mentioned vibration problems. Usually the geometrical parameters that would be beneficial to avoid these vibrations are not optimal from other viewpoints. Thus, the development of stability control algorithms came to the forefront. Several studies investigated active control methods [8–10] to improve the stability of vehicle-trailer combinations, but these are based on in-plane vehicle models. It is also shown in this study, that the linear stability of the straight motion of the trailer is not affected by the pitch motion of the trailer. But a recent result [11] identified a relevant effect on local bifurcations at the stability boundaries.

In this paper, the stability of trailers is analyzed via a spatial four degree-of-freedom mechanical model. All the yaw, pitch and roll motions of the trailer are considered, while the motion of the towing car is imitated by the lateral displacement of the king pin. The model was already used in [11], where the nonlinear vibrations were investigated also taking into account the non-smooth nature of the tire characteristics.

Here, we focus on the linear stability only, but we try to give some hints about the effect of a possible stability control algorithm. A linear feedback control is used to enhance the stability properties of the straight line motion of the trailer. Former studies often use similar or more sophisticated control algorithms, but suppose that the sampling time of the implemented electronic units is small, and the effect of the caused time delay

*Address all correspondence to this author.

is negligible. If the stability control is based on conventional inertial sensors (e.g. accelerometers), this assumption can be valid. When the stability control is based on the new features of an autonomous vehicle (e.g. GPS localization and image processing), the sensor systems can have more relevant time delay although the performance of stability control can be better, see [12]. In our study, this increased time delay of the controller is taken into account, and linear stability charts are constructed ot check its effect on the stability.

The contents of the paper is the following. First, the mechanical model of the trailer is introduced. Then the system is linearised about the straight line motion, for which we also present the equations of motion. Linear stability charts are presented in the plane of the parameters of trailer and the controller. For a specific parameter setup, the effect of the time delay is also shown. Finally, numerical simulation results are presented.

MECHANICAL MODEL

The spatial, 4 degrees-of-freedom (DoF) mechanical model of towed two-wheeled trailers is shown in Fig. 1. Two coordinate systems are differentiated: the ground-fixed coordinate system is denoted by (X,Y,Z), while the (x,y,z) coordinate system is fixed to the trailer itself.

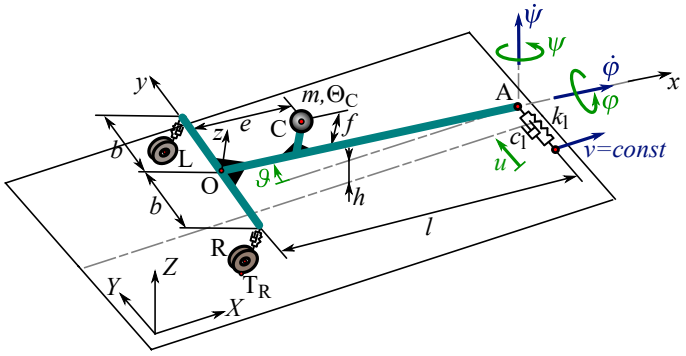

FIGURE 1. THE MECHANICAL MODEL OF TOWED TWO-WHEELED TRAILERS.

The trailer is towed at the king pin A with a constant longitudinal speed v. The mass and the mass moment of inertia is denoted by m and $\mathbf{J}_\mathrm{C}$, respectively. The center of mass is positioned at point C, its horizontal and vertical position can be described with parameters e and f. The vertical distance between the king pin A and the ground is h, the track width is $2b$ and the caster length is l. Points R and L are the center points of the right and the left wheels, respectively. The contact points between the tires and the ground are marked by $\mathrm{T_R}$ and $\mathrm{T_L}$. The stiffness and the damping of the wheel suspensions and the tires are taken into account as an overall stiffness k and an overall damping c. A spring of stiffness k_l and damper of damping c_l are applied to support laterally the king pin at point A, as a representation of the effect of the towing vehicle.

The motion of the trailer can be described with the yaw angle $\psi(t)$, the pitch angle $\vartheta(t)$, the roll angle $\varphi(t)$ and the lateral displacement of the king pin $u(t)$. Thus the system has $n=4$ degrees of freedom, the vector of the generalized coordinates is

$$\mathbf{q}(t) = \left[\psi(t)\ \vartheta(t)\ \varphi(t)\ u(t)\right]^\mathrm{T}. \tag{1}$$

GOVERNING EQUATIONS

Since the system is holonomic, that is there are only geometrical constraints, the equations of motion can be derived with the Lagrange equation of the second kind [13]. For details of the derivation of the governing equations, see [11]. Here, we extend the model of [11] by the effect of the braking forces that are generated by the stability control.

The active forces acting on the trailer are shown in Fig. 2, where $\mathbf{G}$ is the gravitational force; $\mathbf{F}_{\mathrm{R_{tyre}}}$ and $\mathbf{F}_{\mathrm{L_{tyre}}}$ are the tire forces acting at points $\mathrm{T_R}$ and $\mathrm{T_L}$; $\mathbf{F}_{\mathrm{R_{susp}}}$ and $\mathbf{F}_{\mathrm{L_{susp}}}$ are the suspension forces acting on the chassis of the trailer at points R and L; $\mathbf{F}_{\mathrm{A_{lat}}}$ is the lateral force acting at point A; $\mathbf{F}_{\mathrm{R_{brake}}}$ and $\mathbf{F}_{\mathrm{L_{brake}}}$ are the braking forces.

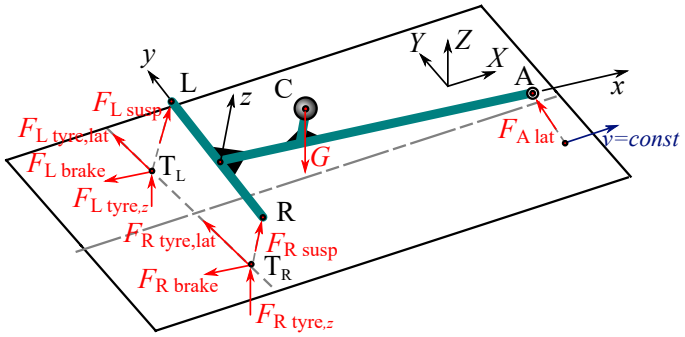

FIGURE 2. THE ACTIVE FORCES ACTING ON THE TRAILER.

The magnitude of the lateral component of the tire forces can be calculated with the help of the so-called Pacejka's Magic Formula [2]. The mass of the wheels is not taken into account, therefore the vertical load on the tires can be calculated from the suspension forces.

For the sake of simplicity, the effect of the braking forces is emulated in our study with the control moment $\mathbf{M}_\mathrm{c}$ acting in the z direction, see Fig. 3. The use of this control moment does not consider all of the effect of the braking forces, namely it does

not influence the pitch motion of the trailer, and it neglects the non-smooth characteristics of the forces that would emerge in the equations of motion. The more precise consideration of these effects will be the tasks of future studies.

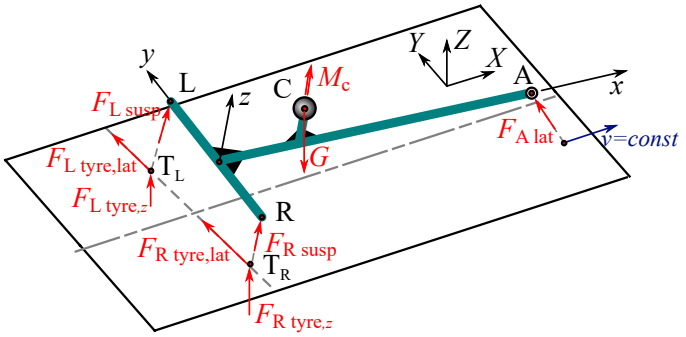

FIGURE 3. THE ACTIVE FORCES ACTING ON THE TRAILER, WHERE THE BRAKING FORCES ARE EMULATED WITH CONTROL MOMENT $\mathbf{M}_c$.

Thus, the control moment is based on the linear feedback:

$$\mathbf{M}_c = \begin{bmatrix} 0 \\ 0 \\ M_c \end{bmatrix}_{(x,y,z)} = \begin{bmatrix} 0 \\ 0 \\ -P\psi(t-\tau) - D\dot{\psi}(t-\tau) \end{bmatrix}_{(x,y,z)}, \quad (2)$$

where τ is the time delay of the control system. The equations of motion can be linearised around the rectilinear motion which corresponds to $\mathbf{q}_0 = \mathbf{0}$, namely

$$\begin{aligned} \psi(t) &\equiv \psi_0 = 0, \\ \vartheta(t) &\equiv \vartheta_0 = 0, \\ \varphi(t) &\equiv \varphi_0 = 0, \\ u(t) &\equiv u_0 = 0. \end{aligned} \quad (3)$$

The linearised equations of motion can be written as

$$\mathbf{M}_{\text{lin}}\ddot{\mathbf{q}}(t) + \mathbf{C}_{\text{lin}}\dot{\mathbf{q}}(t) + \mathbf{K}_{\text{lin}}\mathbf{q}(t) = \mathbf{P}_{\text{lin}}\mathbf{q}(t-\tau) + \mathbf{D}_{\text{lin}}\dot{\mathbf{q}}(t-\tau), \quad (4)$$

where $\mathbf{M}_{\text{lin}}$ is the mass matrix, $\mathbf{C}_{\text{lin}}$ is the damping matrix and $\mathbf{K}_{\text{lin}}$ is the stiffness matrix of the linearised system:

$$\mathbf{M}_{\text{lin}} = \begin{bmatrix} J_{A,z} & 0 & mf(l-e) & -m(l-e) \\ 0 & J_{A,y} & 0 & 0 \\ mf(l-e) & 0 & J_{A,x} & -mf \\ -m(l-e) & 0 & -mf & m \end{bmatrix}, \quad (5)$$

$$\mathbf{C}_{\text{lin}} = \begin{bmatrix} C_1 l & 0 & -C_1 h & -C_1 \\ 0 & 2cl^2 & 0 & 0 \\ -C_1 h & 0 & 2b^2 c + \frac{C_1 h^2}{l} & -\frac{C_1 h}{l} \\ -C_1 & 0 & -\frac{C_1 h}{l} & c_1 + \frac{C_1 h^2}{l} \end{bmatrix}, \quad (6)$$

$$\mathbf{K}_{\text{lin}} = \begin{bmatrix} C_{F\alpha} C_0 & 0 & -C_0 & 0 \\ 0 & 2kl^2 - mgf & 0 & 0 \\ -\frac{C_{F\alpha} C_0 h}{l} & 0 & 2kb^2 - mgf & 0 \\ -\frac{C_{F\alpha} C_0 h}{l} & 0 & -\frac{C_0}{l} & k_1 \end{bmatrix}, \quad (7)$$

where

$$C_{F\alpha} = B_m C_m D_m \quad (8)$$

is the so-called cornering stiffness, where B_m, C_m and D_m are the stiffness, shape and peak factors of the Magic Formula. We also introduce

$$C_0 = mg(l-e) \quad \text{and} \quad C_1 = \frac{C_{F\alpha} C_0}{v} \quad (9)$$

in order to shorten the formulas. The matrices corresponding to the control moment are the following:

$$\mathbf{P}_{\text{lin}} = \begin{bmatrix} -P & 0 & 0 & 0 \\ 0 & 0 & 0 & 0 \\ 0 & 0 & 0 & 0 \\ 0 & 0 & 0 & 0 \end{bmatrix}, \quad \mathbf{D}_{\text{lin}} = \begin{bmatrix} -D & 0 & 0 & 0 \\ 0 & 0 & 0 & 0 \\ 0 & 0 & 0 & 0 \\ 0 & 0 & 0 & 0 \end{bmatrix}. \quad (10)$$

As it can be seen, the linearised system can be separated into two subsystems: one differential equation can be disjointed, namely the pitch motion can be analyzed alone (1 DoF subsystem), while the remaining equations are coupled (3 DoF subsystem).

By using exponential trial function

$$\mathbf{q}(t) = \mathbf{A}e^{\lambda t} \quad (11)$$

in Eqn. (4), we obtain:

$$\left(\mathbf{M}_{\text{lin}}\lambda^2 + \mathbf{C}_{\text{lin}}\lambda + \mathbf{K}_{\text{lin}}\right)\mathbf{A}e^{\lambda t} = \left(\mathbf{P}_{\text{lin}} + \mathbf{D}_{\text{lin}}\lambda\right)\mathbf{A}e^{\lambda(t-\tau)}. \quad (12)$$

This can be rearranged as

$$\left(\mathbf{M}_{\text{lin}}\lambda^2 + \mathbf{C}_{\text{lin}}\lambda + \mathbf{K}_{\text{lin}} - \left(\mathbf{P}_{\text{lin}} + \mathbf{D}_{\text{lin}}\lambda\right)e^{\lambda(-\tau)}\right)\mathbf{A} = \mathbf{0}. \quad (13)$$

TABLE 1. PARAMETER VALUES OF THE TRAILER.

Notation	Parameter	Value
l	caster length	3 m
b	half of the track width	0.8 m
h	height of the king pin	0.5 m
e	horizontal position of CG	0.9 m
f	vertical position of CG	1 m
m	mass of the trailer	3000 kg
k	stiffness of the suspension	60 kN/m
c	damping of suspension	6 kNs/m
k_l	lateral stiffness	10 kN/m
c_l	lateral damping	100 Ns/m
B_m	stiffness factor	10
C_m	shape factor	1.9
D_m	peak factor	1
E_m	curvature factor	0.97

The characteristic function of the system can be calculated as the determinant of the coefficient matrix, namely:

$$D_{\mathrm{char}}(\lambda) := \det\left(\mathbf{M}_{\mathrm{lin}}\lambda^2 + \mathbf{C}_{\mathrm{lin}}\lambda + \mathbf{K}_{\mathrm{lin}} - (\mathbf{P}_{\mathrm{lin}} + \mathbf{D}_{\mathrm{lin}}\lambda)\,\mathrm{e}^{\lambda(-\tau)}\right) \tag{14}$$

Due to the presence of the time delay, the characteristic equation $D_{\mathrm{char}}(\lambda) = 0$ is transcendental, but the stability boundaries can be determined, where pure complex characteristic roots exist. Here, we use the D-subdivision method, namely $\lambda = \mathrm{i}\omega$ is substituted into Eqn. (14) and the real and imaginary parts are separated:

$$\begin{aligned} \mathrm{Re}(D_{\mathrm{char}}(\mathrm{i}\omega)) &= 0\,, \\ \mathrm{Im}(D_{\mathrm{char}}(\mathrm{i}\omega)) &= 0\,. \end{aligned} \tag{15}$$

In case of our system, the boundaries cannot be calculated analytically, but it can be analyzed numerically. The Eqns. (15) can be solved for example with the help of the *Multidimensional Bisection Method* [14] for a specific range of two system parameters meantime the angular frequency ω is swept.

THE EFFECT OF TIME DELAY ON LINEAR STABILITY

The effects of the stability control are investigated for a specific parameter setup shown in Tab. 1. In Fig. 4, linear stability charts are plotted in the plane of the vertical position f of the center of gravity and the towing speed for different time delays. The panels of each figures are plotted for different P and D control parameter values. The thick black, blue and grey lines correspond to the linear stability boundaries. The linearly stable (S) and unstable (U) regions are also marked.

For the case when there is no time delay $\tau = 0$ (see the continuous black line in Fig. 4), it can be seen, the linearly unstable region decreases when the values of the control gains are increased.

Having even small time delay in the system $\tau = 0.05$ s, the linearly unstable region increases relative to the zero time delay case, see the continuous blue line in Fig. 4. But the use of the stability control is beneficial, namely linearly unstable region shrinks as the control gains are increased.

When the time delay is greater, namely when $\tau = 0.1$ s is set, and the proportional gain P is increased, the linearly unstable region grows, see the grey line in Fig. 4. On the contrary, the increase of the derivative gain in the investigated parameter range remains advantageous with respect to the stability properties.

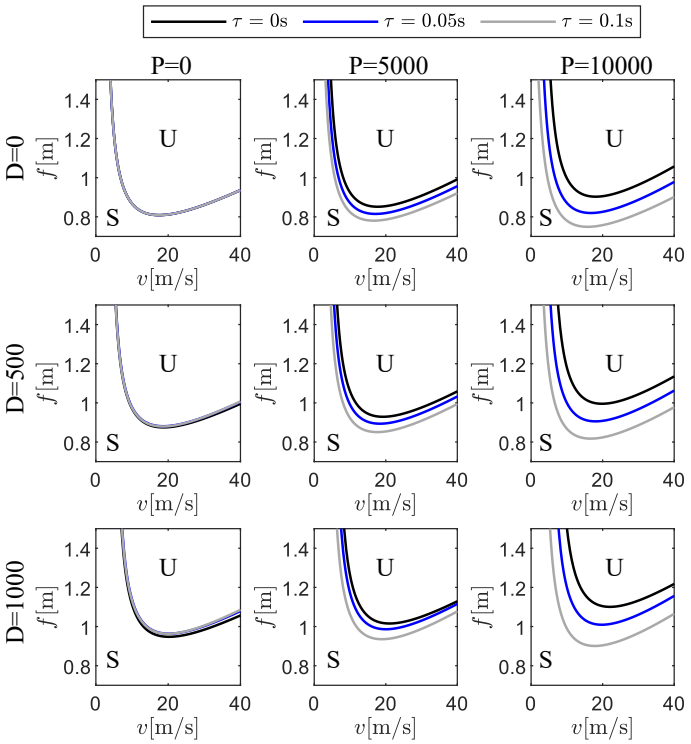

FIGURE 4. THE STABILITY CHARTS FOR DIFFERENT P AND D CONTROL PARAMETER VALUES AND FOR $\tau = 0$ s (BLACK LINE), $\tau = 0.05$ s (BLUE LINE) AND $\tau = 0.1$ s (GREY LINE).

To analyze the stability of the control, one can also deter-

mine the critical values for the control gains for a specific setup of the trailer. Figure 5 shows the stability boundaries of the linearised system in the plane of the proportional P and the derivative D gains for $\tau = 0.1$ s. In the figure, we use the parameters $f = 1$ m and $v = 20$ m/s. The stability boundary is plotted for $\omega \in [0, 100]$ rad/s. One can observe the static stability boundary ($\omega = 0$) at approximately $P = -92000$ Nm, see the vertical line in the figure. Below this proportional gain value a positive real characteristic root exists. To determine the stability properties of the different regions of the stability chart one can use the semi-discretization [15], for example. This is a future task of our study. However, the stability properties can be checked with numerical simulations, too. In the figure, the light grey and white areas correspond to linearly unstable and stable domains, respectively.

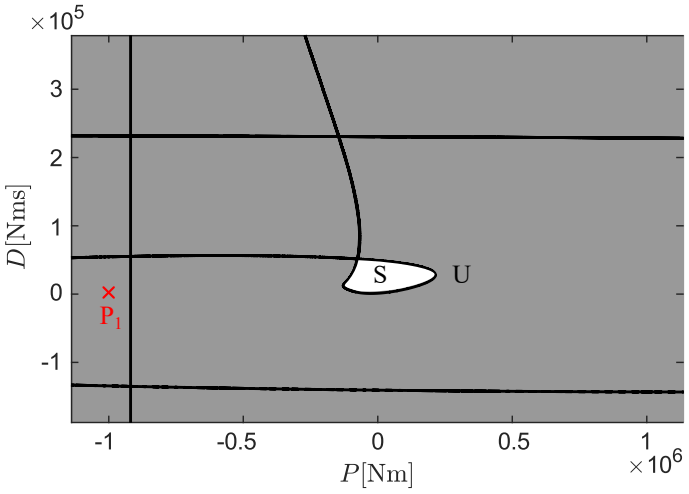

FIGURE 5. THE STABILITY BOUNDARIES IN THE PLANE OF THE CONTROL GAINS FOR $f = 1$ m, $v = 20$ m/s AND $\tau = 0.1$ s.

The stability charts can be shown for a more relevant control parameter ranges, see Fig. 6. In the panels, the light grey and white areas correspond to linearly unstable and stable domain, respectively. For the time delay free case $\tau = 0$, the stability properties of the different regions were determined. For the non-zero delay case, we assume that the presence of a small time delay does not change the pattern of the stability regions. Therefore, the linearly stable and unstable domains are also shown for $\tau = 0.05$ s and $\tau = 0.1$ s, see the middle and bottom panel of Fig. 6. As can be seen, the linearly unstable domain is much greater in the examined region for larger time delay, as was expected.

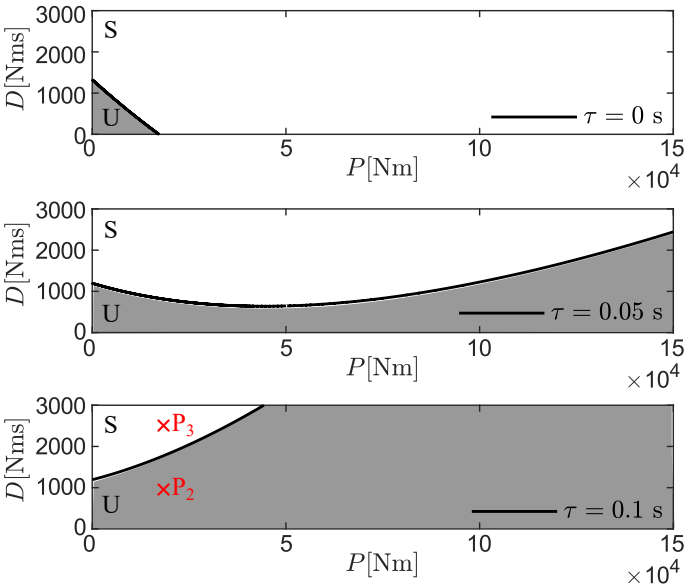

FIGURE 6. THE STABILITY CHARTS FOR $\tau = 0$ s, $\tau = 0.05$ s AND $\tau = 0.1$ s.

NUMERICAL SIMULATIONS

The stability properties of certain points can be checked by means of numerical simulations. The equations of motion are rewritten in first order form:

$$\begin{bmatrix}\dot{\mathbf{q}}(t)\\ \ddot{\mathbf{q}}(t)\end{bmatrix} = \begin{bmatrix}\mathbf{0} & \mathbf{I}\\ -\mathbf{M}_{\text{lin}}{}^{-1}\mathbf{K}_{\text{lin}} & -\mathbf{M}_{\text{lin}}{}^{-1}\mathbf{C}_{\text{lin}}\end{bmatrix}\begin{bmatrix}\mathbf{q}(t)\\ \dot{\mathbf{q}}(t)\end{bmatrix} + \begin{bmatrix}\mathbf{0} & \mathbf{0}\\ \mathbf{M}_{\text{lin}}{}^{-1}\mathbf{P}_{\text{lin}} & \mathbf{M}_{\text{lin}}{}^{-1}\mathbf{D}_{\text{lin}}\end{bmatrix}\begin{bmatrix}\mathbf{q}(t-\tau)\\ \dot{\mathbf{q}}(t-\tau)\end{bmatrix}, \tag{16}$$

which can be written as

$$\dot{\mathbf{y}}(t) = \mathbf{A}\mathbf{y}(t) + \mathbf{B}\mathbf{y}(t-\tau). \tag{17}$$

DDE23 was used with the initial condition $\mathbf{y}(t) = \mathbf{0}$ for $t \in [-\tau, 0)$ and $\mathbf{y}(0) = \begin{bmatrix}0\ 0\ 0\ 0\ \Omega_0\ 0\ 0\ 0\end{bmatrix}^{\mathrm{T}}$, where $\dot{\psi}(0) = \Omega_0 = 0.1$ rad/s was applied as an impact-like perturbation. The time graphs of the generalized coordinates can be seen in Fig. 7, 8 and 9 for $f = 1$ m, $v = 20$ m/s and $\tau = 0.1$ s. In the figures $\vartheta(t) \equiv 0$ since the linearized governing equations are simulated in which the pitch motion is decoupled (see Eqn. (4)).

Static loss of stability can be seen in Fig. 7, which corresponds to parameter point P_1 in Fig. 5. That is, the trailer loses its stability without oscillations due to the fact that the system has a positive real characteristic root.

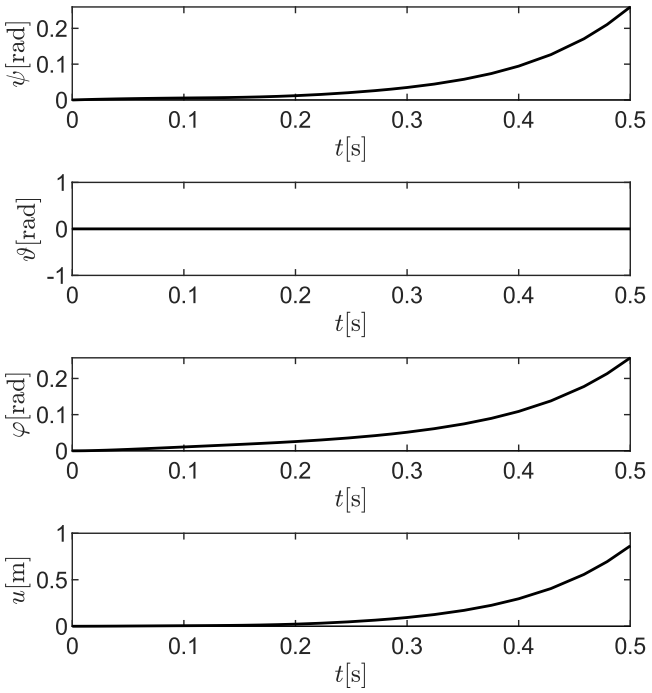

FIGURE 7. THE TIME GRAPHS OF THE GENERALIZED COORDINATES FOR $\tau = 0.1$ s, $P = -100000$ Nm AND $D = 1000$ Nms (STATIC LOSS OF STABILITY).

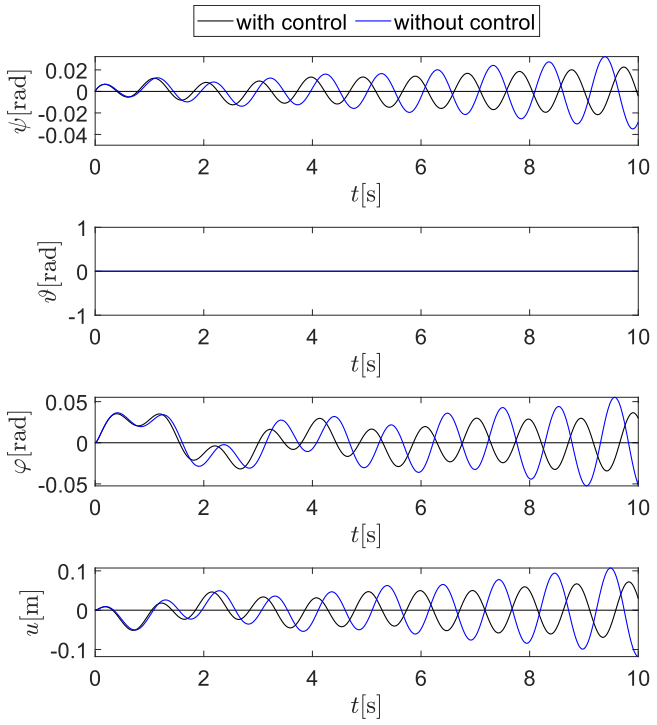

FIGURE 8. THE TIME GRAPHS OF THE GENERALIZED COORDINATES FOR $\tau = 0.1$ s, WITH CONTROL ($P = 20000$ Nm AND $D = 1000$ Nms) AND WITHOUT CONTROL (DYNAMIC LOSS OF STABILITY).

The trailer loses its stability via oscillations if the control gains are $P = 20000$ Nm and $D = 1000$ Nms, see the black continuous lines in Fig. 8, which corresponds to parameter point P_2 in Fig. 6. The oscillations without control can be seen with blue continuous lines. The effect of the impact-like initial perturbation in the yaw rate $\dot{\psi}(t)$ excites all the vibration modes of the system that can be observed in the first half of the time graphs. As can be seen, the oscillations are reduced by introducing the control.

By increasing the value of the proportional gain P for fixed $D = 1000$ Nms, the motion becomes stable above a certain value. An example for a stable motion is shown with black continuous lines in Fig. 9, which corresponds to parameter point P_3 in Fig. 6. The oscillations without control can be seen with blue continuous lines. As can be seen, the otherwise unstable motion is stabilized with the help of the control.

CONCLUSIONS

A spatial model of two-wheeled trailers was introduced to analyze the stability of car-trailer systems. The effect of a possible stability control was emulated by a control torque that is generated by the braking forces. Our approach only considers the effect of the control on the yaw dynamics, and do not take into account the direct effect of the braking forces on the pitch motion. Moreover, in real case, the non-smooth characteristics of the braking forces can be relevant when the nonlinear oscillations are investigated.

However, some stability charts were shown and used to give some impression about the effect of the controller and the time delay. For a specific parameter setup, we showed that detailed analysis of the linear stability is necessary to determine the appropriate control gains when the time delay is large. More detailed and precise analysis is the task of our future work.

ACKNOWLEDGMENT

This research was partly supported by the National Research, Development and Innovation Office under grant no. NKFI-128422 and by the Higher Education Excellence Program of the Ministry of Human Capacities in the frame of Artificial intelligence research area of Budapest University of Technology and Economics (BME FIKP-MI).

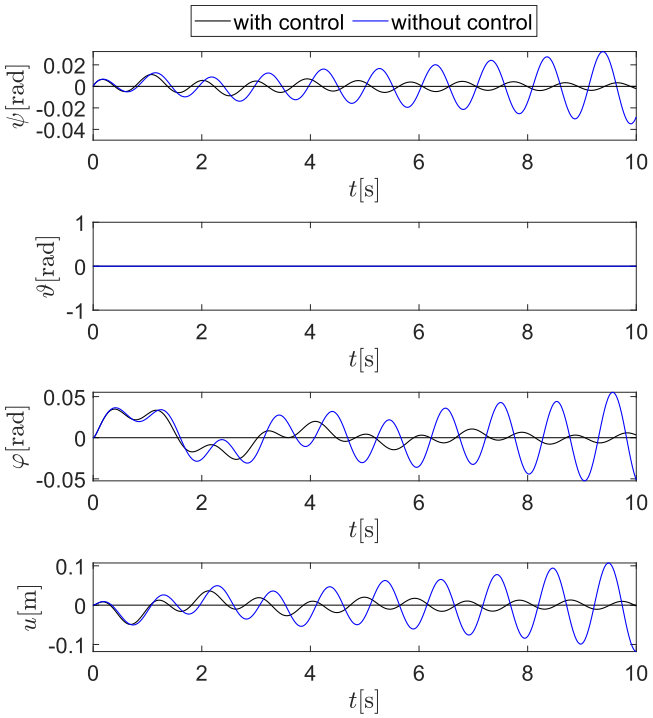

FIGURE 9. THE TIME GRAPHS OF THE GENERALIZED COORDINATES FOR $\tau = 0.1$ s, WITH CONTROL ($P = 20000$ Nm AND $D = 2500$ Nms) AND WITHOUT CONTROL (STABLE MOTION).

REFERENCES

[1] Schlippe, B., and Dietrich, R., 1941. "Das Flattern Eines Bepneuten Rades (Shimmying of a pneumatic wheel)". In Bericht 140 der Lilienthal-Gesellschaft für Luftfahrtforschung, pp. 35–45, 63–66. English translation is available in *NACA Technical Memorandum* 1365, pages 125-166, 217-228, 1954.

[2] Pacejka, H., 2002. *Tyre and Vehicle Dynamics*. Elsevier Butterworth-Heinemann.

[3] Sharp, R. S., Evangelou, S., and Limebeer, D. J. N., 2004. "Advances in the modelling of motorcycle dynamics". *Multibody System Dynamics,* ***12***(3), pp. 251–283.

[4] Troger, H., and Zeman, K., 1984. "A nonlinear-analysis of the generic types of loss of stability of the steady-state motion of a tractor-semitrailer". *Vehicle System Dynamics,* ***13***(4), pp. 161–172.

[5] Darling, J., Tilley, D., and Gao, B., 2009. "An experimental investigation of car–trailer high-speed stability". *Proceedings of the Institution of Mechanical Engineers, Part D: Journal of Automobile Engineering,* ***223***(4), pp. 471–484.

[6] Beregi, S., Takacs, D., Gyebroszki, G., and Stepan, G., 2019. "Theoretical and experimental study on the nonlinear dynamics of wheel-shimmy". *Nonlinear Dynamics,* ***98***, pp. 2581–2593.

[7] Sharp, R. S., and Fernańdez, M. A. A., 2002. "Car-caravan snaking - part 1: the influence of pintle pin friction". In Proceedings of the Institution of Mechanical Engineers Part C - Journal of Mechanical Engineering Science, Vol. 216 of *7*, pp. 707–722.

[8] Hac, A., Fulk, D., and Chen, H., 2008. "Stability and control considerations of vehicle-trailer combination". *SAE International*.

[9] Kageyama, I., and Nagai, R., 1995. "Stabilization of passenger car-caravan combination using four wheel steering control". *Vehicle System Dynamics,* ***24***(4-5), pp. 313–327.

[10] Deng, W., Lee, Y. H., and Tian, M., 2004. "An integrated chassis control for vehicle-trailer stability and handling performance". *SAE Technical Paper Series*.

[11] Horvath, H. Z., and Takacs, D., 2020. "Analogue models of rocking suitcases and snaking trailers". *Nonlinear Dynamics of Structures, Systems and Devices*, pp. 117–126.

[12] Olofsson, B., and Nielsen, L., 2020. "Using crash databases to predict effectiveness of new autonomous vehicle maneuvers for lane-departure injury reduction". *IEEE Transactions on Intelligent Transportation Systems*, pp. 1–12.

[13] Gantmacher, F., 1975. *Lectures in analytical mechanics*. MIR Publishers, Moscow.

[14] Bachrathy, D., and Stepan, G., 2012. "Bisection method in higher dimensions and the efficiency number". *Periodica Polytechnica - Mechanical Engineering,* ***56***(2), pp. 81–86.

[15] Insperger, T., and Stepan, G., 2011. *Semi-Discretization for Time-Delay Systems*. Springer New York, pp. 39–71.